IEEE Open Access Journal of
Power and Energy

Received 2 November 2023; revised 28 January 2024; accepted 13 February 2024.
Date of publication 26 February 2024; date of current version 28 March 2024.

Digital Object Identifier 10.1109/OAJPE.2024.3370504

Frequency Nadir Constrained Unit Commitment for High Renewable Penetration Island Power Systems

XUEBO LIU[1,2] (Graduate Student Member, IEEE), XIN FANG[3] (Senior Member, IEEE), NINGCHAO GAO[1] (Graduate Student Member, IEEE), HAOYU YUAN[4] (Member, IEEE), ANDY HOKE[1] (Senior Member, IEEE), HONGYU WU[2] (Senior Member, IEEE), AND JIN TAN[1] (Senior Member, IEEE)

[1]National Renewable Energy Laboratory (NREL), Golden, CO 80401 USA
[2]Mike Wiegers Department of Electrical and Computer Engineering, Kansas State University, Manhattan, KS 66502 USA
[3]Department of Electrical and Computer Engineering, Mississippi State University, Starkville, MS 39762 USA
[4]Active Power Investments LLC, Bellaire, TX 77401 USA

CORRESPONDING AUTHOR: J. TAN (Jin.Tan@nrel.gov)

This work was supported in part by the National Renewable Energy Laboratory, operated by Alliance for Sustainable Energy, LLC, under U.S. Department of Energy (DOE) under Contract DE-AC36-08GO28308, and in part by the U.S. Department of Energy Office of Energy Efficiency and Renewable Energy, Solar Energy Technologies Office under Grant 34224 and Grant 37772.

ABSTRACT The process of energy decarbonization in island power systems is accelerated due to the swift integration of inverter-based renewable energy resources (IBRs). The unique features of such systems, including rapid frequency changes resulting from potential generation outages or imbalances due to the unpredictability of renewable power, pose a significant challenge in maintaining the frequency nadir without external support. This paper presents a unit commitment (UC) model with data-driven frequency nadir constraints, including either frequency nadir or minimum inertia requirements, helping to limit frequency deviations after significant generator outages. The constraints are formulated using a linear regression model that takes advantage of real-world, year-long generation scheduling and dynamic simulation data. The efficacy of the proposed UC model is verified through a year-long simulation in an actual island power system using historical weather data. The alternative minimum inertia constraint, derived from actual system operation assumptions, is also evaluated. Findings demonstrate that the proposed frequency nadir constraint notably improves the system's frequency nadir under high photovoltaic (PV) penetration levels, albeit with a slight increase in generation costs, when compared to the alternative minimum inertia constraint.

INDEX TERMS Linear regression, frequency nadir, unit commitment, renewable integration, island system.

NOMENCLATURE

Indices

b	Index for load buses.
i	Index for generation units.
p	Index for photovoltaic (PV) generation units.
t	Index for time interval.
T	Time span.
l	Index for transmission lines.

Constants

H_i	Inertia of unit i.
SU_i	Startup cost of unit i.
SD_i	Shutdown cost of unit i.
R_i^U	Ramp-up limit for unit i.
R_i^D	Ramp-down limit for unit i.
R_i^{SU}	Ramp-up limit for unit i when starting up.
R_i^{SD}	Ramp-down limit for unit i when shutting down.
$Limit_l$	Transmission limit for line l.
$\overline{D_{b,t}}$	Forecasted power demand mean value of load bus b at time t.
$\overline{P_{p,t}}$	Forecasted PV power (maximum power point tracking) of unit p at time t.
$G_{i,t}^{max}$	Maximum generation output of unit i at time t.
$G_{i,t}^{min}$	Minimum generation output of unit i at time t.

$T_{i,MinUp}$	Minimum uptime (MUT) for unit i.
$T_{i,MinDn}$	Minimum downtime (MDT) for unit i.
GSF_{l-i}	Generation shift factor from bus i to line l .
LP	Price of load-shedding penalty.
H	Total inertia of the system.
$RP/\ PFP$	Regulation reserve and primary frequency reserve shortage penalty price.
PFR_t^r	Primary frequency reserve requirement at time t.
$Reg_{u,t}^r$	Regulation-up reserve requirement at time t.
$Reg_{d,t}^r$	Regulation-down reserve requirement at time t.

Variables

$cp_{i,t}$	Production cost for unit i at time t.
$G_{i,t}$	Generation output for unit i at time t .
$\overline{G_{i,t}}$	Maximum available generation output for unit i at time t.
$P_{p,t}$	PV power output for unit p at time t.
$D_{b,t}$	Scheduled demand for the bus b at time t.
$\Delta D_{b,t}$	Load-shedding quantity of bus b at time t.
ΔPFR_t	Capacity shortage in the system PFR at time t.
ΔD_t	System load shedding at time t.
$\Delta Reg_{u,t}$	System regulation-up shortage at time t.
$\Delta Reg_{d,t}$	System regulation down shortage at time t.
$Reg_{u,i,t}$	Regulation-up capacity provided by unit i at time t.
$Reg_{d,i,t}$	Regulation-down capacity provided by unit i at time t.
$Reg_{u,p,t}$	Regulation-up capacity provided by PV power plant p at time t.
$Reg_{d,p,t}$	Regulation-down capacity provided by PV power plant p at time t.
$PFR_{i,t}$	PFR capacity of unit i at time t.
$v_{i,t}$	Commitment status of unit i at time t.
$u_{i,t}$	Startup status of the unit i at time t.
$w_{i,t}$	Shutdown status of unit i at time t.

I. INTRODUCTION

INVERTER-BASED resources (IBRs) deployed for energy decarbonization in power systems pose challenges to stabilizing system frequency due to the absence of conventional rotational inertia support [1], [2]. Variability and uncertainty in IBR power outputs exacerbate power imbalances, leading to larger frequency excursions and increased resource requirements for frequency regulation [3], [4]. Replacement of conventional generators with IBR reduces system inertia and the reliability of frequency regulation. Consequently, power systems with high renewable penetration face a lower frequency nadir, risking under-frequency load shedding (UFLS) [5], [6] after generation tripping. This urgent issue is particularly critical for island systems without interconnection. Some system operators in the United Kingdom adopt a minimum inertia constraint approach [7], used in power systems with significant penetration of IBR, which has the drawback of increasing cost. Maintaining conventional generators online solely for inertia support incurs additional expenses for maintenance, fuel, and operations. As the IBR share increases, reliance on costly conventional generators for the inertia response grows, posing financial challenges and questioning the long-term feasibility of this approach.

To maintain frequency stability in the system operation stage, researchers integrate the frequency nadir constraint into a traditional generation scheduling problem, such as unit commitment (UC) and economic dispatch (ED). A comprehensive literature review, presented in Table 1, reveals that the frequency nadir constraints can be derived from two approaches: the analytical model method [1], [8], [9], [10], [11], [12], [13], [14], [15], [16], [17], [18], [19], [20], [21] and the data-driven method [22], [23], [24], [25], [26], [27], [28], [29]. However, incorporating the frequency nadir constraint into existing Mixed Integer Linear Programming (MILP)-based UC problem through either of these methods, particularly the data-driven approach, can increase the Complexity of Adaption (CoA), leading to a larger number of decision variables and parameters during linearization or master-sub programming, and hence can increase computational complexity. Categorically, we conclude three challenges to incorporating frequency nadir constraints to MILP-based UC problems in the current situation:

First, the non-linearity of the nadir constraints makes it challenging to incorporate them into a MILP-based UC model. Many studies use Piece Wise Linear (PWL) [1], [8], [9], [11], [12], [13], [14], [15], [16], [17], [19] and Benders' Decomposition (BD) [18], [22], [23], [24], [25] methods to integrate the constraint. Piecewise linearization allows for the representation of nonlinear functions with a series of linear segments, offering more flexibility in modeling complex relationships. However, using PWL requires careful selection of breakpoints and can lead to a high approximate error, while using BD could result in infeasible solutions in subproblems. These methods can increase CoA in the MILP-based UC problem by introducing more decision variables and parameters during linearization. A frequency nadir constraint has a small CoA in MILP when it is closer to a linear equation, while a nonlinear frequency nadir constraint leads to a higher CoA in MILP. Moreover, those constraints with higher CoA result in higher computational complexity during linearization.

Second, accurately estimating the frequency nadir constraint is essential to maintain adequate inertia and headroom for fast frequency response, as well as to ensure that the system frequency nadir remains within acceptable limits [30]. However, accurately estimating this constraint is challenging due to various factors such as inertia, synchronous reactance, time constants, droop settings of conventional generators and IBRs, and the number of online units. Analytical models may not capture all the nonlinear relationships involved, further complicating the estimation process. Fortunately, data-driven methods [22], [23], [24], [25], [26], [27], [28], [29] can offer accurate estimates by treating the frequency nadir and the input data as black boxes, considering the entire system and its output. These data-driven approaches provide a viable alternative to analytical models, leveraging the advantages of capturing complex nonlinear relationships. Therefore, this work embraces the benefits of data-driven models to estimate

TABLE 1. Comparison of related works in the literature (in publication time order).

Reference	Frequency constraint	Real sys. w/ High IBR	Approaches	Validation Period	CoA
[8]/2013	Analytical-model	✓	Piece Wise Linear	24 hours	Mid
[9]/2014	Analytical-model		Piece Wise Linear	6 hours	Mid
[10]/2016	Analytical-model	✓	Ordinary Differential Equation	6 hours	Mid
[11]/2016	Analytical-model		Piece Wise Linear	24 hours	Mid
[12]/2016	Analytical-model	✓	Piece Wise Linear	146 hours	Mid
[22]/2016	Data-driven		CSC-based Benders' Decomposition	24 hours	High
[23]/2019	Data-driven		CSC-based Benders' Decomposition	24 hours	High
[24]/2019	Data-driven		Duality-Free Benders' Decomposition	24 hours	High
[13]/2019	Analytical-model	✓	Piece Wise Linear	8760 hours	Mid
[1]/2019	Analytical-model		Piece Wise Linear	24 hours	Mid
[14]/2019	Analytical-model	✓	Piece Wise Linear	48 hours	Mid
[15]/2020	Analytical-model		Piece Wise Linear	24 hours	Mid
[16], [17]/2021	Analytical-model		Piece Wise Linear	24 hours	Mid
[31]/2021	Analytical-model	✓	Adaptive Piece Wise Linear	24 hours	Mid
[18]/2021	Analytical-model	✓	Bilinear Benders' Decomposition	24 hours	High
[25]/2021	Data-driven		OCT-based Benders' Decomposition	24 hours	High
[19]/2022	Analytical-model		Piece Wise Linear	24 hours	Mid
[20]/2022	Analytical-model	✓	Tri-level Benders' Decomposition	24 hours	High
[21]/2022	Analytical-model		Gauss–Seidel Iterations	40 seconds	High
[26]/2022	Data-driven		DNN-based Binary Encoder	24 hours	High
[27]/2022	Data-driven		Wasserstein-Metric Ambiguity Set	24 hours	High
[28]/2022	Data-driven		SVR-based Linearization	24 hours	Mid
[29]/2022	Data-driven	✓	Logistic Regression	24 hours	Mid
This work	Data-driven	✓	Linear Regression	8760 hours	Low

the frequency nadir instead of relying solely on analytical models.

Third, validation and testing of the frequency nadir constraint is crucial to ensure its accuracy, reliability, and effectiveness in the MILP solution. Long-term simulations with realistic time series data and real-world systems are necessary for comprehensive validation under various system operation scenarios. Most studies use a simulation of one day (24 hours) [1], [8], [9], [11], [14], [15], [16], [17], [18], [19], [22], [23], [24], [25]. The volatile operation conditions of high-IBR penetration power systems, including the impact of large-capacity PV-battery systems and their operating hours, cannot be fully satisfied with his short-term validation. Therefore, a ''long-term'' simulation with attentive analysis is crucial to confirm the frequency nadir constraint's effectiveness while considering dynamic performance.

Thus, to solve the aforementioned challenges of incorporating the frequency nadir constraint into MILP of the unit commitment problem with efficiency and easy applicability by industry considered, this study proposes a novel data-driven frequency nadir-constrained unit commitment (FNC-UC) model, which imposes constraints on frequency nadir following the largest generation contingency. The main contributions can be summarized below:

1) A data-driven, linear regression-based frequency nadir estimation model is proposed that accounts for the impacts of the system inertia, the headroom for the primary frequency response (PFR), and the largest generator's output capacity in a generation trip contingency. Based on our previous study [32], this model provides a highly accurate estimate of the frequency nadir in a realistic island system with a generation-tripping contingency.
2) The proposed frequency nadir model is embedded in a MILP-based unit commitment formulation such that the system frequency nadir after the most significant generator outage is endogenously considered in the generation dispatch problem. It should be noted that the proposed FNC-UC model has a lower CoA compared to previous studies, as shown in Table 1, making it both computationally efficient and easily applicable in the industry.
3) A real-world island system with high IBR penetration, Maui Island Grid, with realistic load and renewable generation profiles, is used to validate the proposed FNC-UC model. The proposed FNC-UC is comprehensively validated over a long-term period, effectively demonstrating its performance. In addition, the economic and reliability impacts of the proposed frequency nadir constraints on Maui Island operation are quantified.

The remainder of this paper is organized as follows. The regression-based linear frequency nadir constraint is introduced in Section II. The procedure to obtain this linear constraint is also presented. The FNC-UC model that contains the frequency nadir or minimum-inertia requirement constraints is formulated in Section III. Case studies in an island system are performed and analyzed in Section IV. Section V concludes the paper.

II. DATA-DRIVEN DYNAMIC FREQUENCY NADIR CONSTRAINT

This section introduces the procedure for obtaining the linear frequency nadir constraint through a linear regression model with an extensive historical load of one year, renewable power generation scheduling, and dynamic simulations. The data-driven-based nadir estimation and the proposed FNC-UC framework will be introduced in Subsections II-A and II-B.

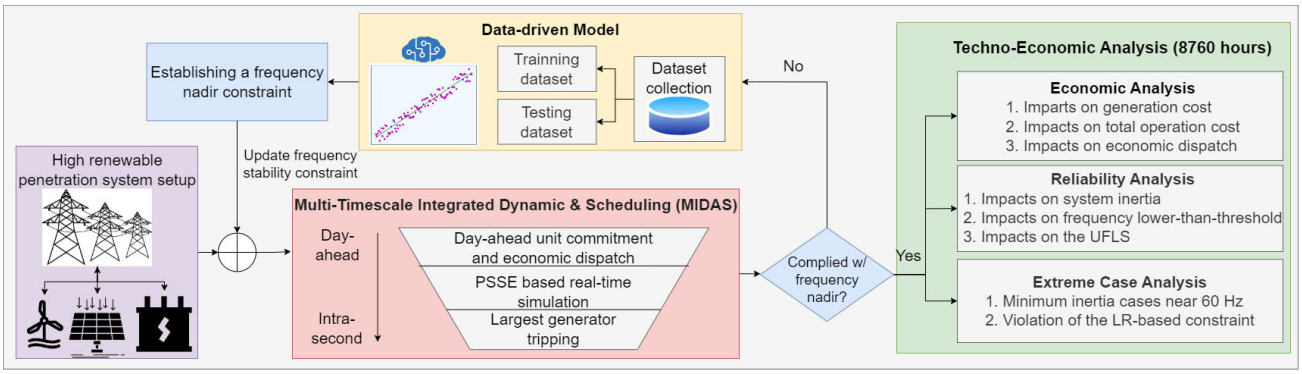

FIGURE 1. Illustration of the proposed frequency nadir constraint unit commitment approach.

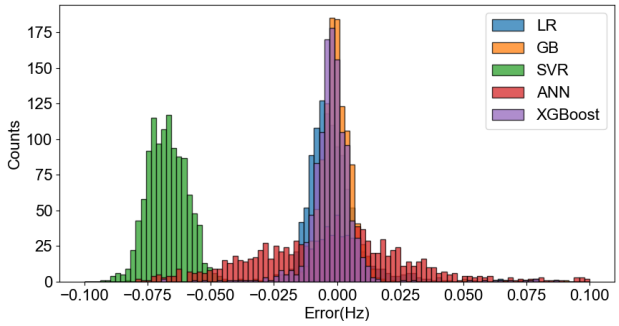

FIGURE 2. Total inertia and headroom dataset testing error distribution [32].

A. DATA DRIVEN-BASED FREQUENCY NADIR ESTIMATION

In our previous study [32], we evaluated five data-driven methods (linear regression (LR), gradient boosting (GB), support vector regression (SVR), artificial neural network (ANN), and XGBoost to predict frequency nadir in the power system with high renewable penetration levels. The training and testing dataset is Total Inertia Headroom (TIH), which was generated using simulations with the Multi-Timescale Integrated Dynamic and Scheduling (MIDAS) [33], [34] toolbox. The attributes in the TIH dataset include the system-wide inertia and the PFR headroom. The results showed that the five methods had a high prediction accuracy. In particular, linear regression ranked higher than ANN and SVR, as shown in Fig. 2. Although LR may not have the best error performance, it can still provide reasonable accuracy after considering CoA. The hourly total inertia and total headroom can be calculated as follows:

$$Inertia_t = \sum_{i=0}^{N} v_{i,t} \cdot H_i \cdot \text{Mbase}_i, \forall i$$
$$PFR_t^{headroom} = \sum_{i=0}^{N} (\overline{G_{i,t}} - G_{i,t}), \forall i \quad (1)$$

where $Inertia_t$ and $PFR_t^{headroom}$ are the systems total inertia (MW*s) and total headroom (MW) at time t; H_i is the inertia of unit i; Mbase_i is the rating in MVA of unit i; $\overline{G_{i,t}}$ and $G_{i,t}$ are the maximum generation and the power generation of unit i at time t, respectively. Inspired by [35], [36], and [37], which is typically used to analyze the frequency nadir of connected machines in the entire system, the swing equation in the DC model can be simplified as

$$Inertia \cdot \frac{2\partial \Delta f(t)}{\partial t} = PFR^{headroom} - \Delta P_L \quad (2)$$

where ΔP_L is the power outage, $\Delta f(t)$ is the frequency deviation function of t. Therefore, it is significant to consider potential power outages as an element in the frequency nadir constraint to ensure the power system maintains the frequency above the threshold of the UFLS level. Most studies [12], [13], [36], and [37] use the largest generation outage for this P_L.

Linear regression is one of the most common techniques in machine learning [38]. Extensive literature [39], [40] shows that linear regression performs well in forecasting, prediction, and classification applications. It can provide stable, robust, and accurate prediction results. The goal of linear regression is to build a model whose output scalar, $y \in \mathbb{R}$, is a linear function of the input vector, $x \in \mathrm{R}^n$, by solving a regression problem. Let $\hat{y}$ be the prediction value and y be the actual value, so the equation of the linear regression should be defined as $\hat{y} = \mathbf{w}^{\mathrm{T}}\mathbf{x} + b$, where $\mathbf{w}^{\mathrm{T}} \in \mathrm{R}^n$ is the vector of parameters; b is an intercept term. Note that the parameters are values that control the prediction of the system. In other words, the output, $\hat{y}$, is the sum of all the weighted input vectors, $\mathbf{x}$. The more significant weight, w^i, contributes more substantially to the prediction value. The training process is listed as follows:

$$\frac{1}{n}\nabla_w\Big[\sum_{i=1}^{n}(y_i^{train} - \hat{y}_i^{train})^2\Big] = 0$$
$$\nabla_{\mathbf{w}}(\mathbf{X}^{train}\mathbf{w} - \mathbf{y}^{train})^{\mathrm{T}}(\mathbf{X}^{train}\mathbf{w} - \mathbf{y}^{train}) = 0 \quad (3)$$

In a nutshell, considering an N-1 largest generation contingency (tripping the largest generation), the inertia of the system, the amount of headroom, and the largest power generation are the most related variables in the linear regression equation to estimate the frequency nadir of the system. The

adopted formulation from the linear regression to this study is the linear regression-based nadir constraint in (4), as shown:

$$f_{nadir} = a * Inertia + b * PFR_{headroom} + c * P_{max} + d \quad (4)$$

where f_{nadir} is the frequency nadir (Hz); P_{max} is the system's largest generation outage capacity (MW); and a, b, c and d are the linear coefficients obtained from linear regression. In our previous study [32], we analyzed the impact of inertia and PFR headroom on frequency nadir in power systems. Traditional systems exhibit a strong correlation with inertia and a weak correlation with PFR due to its slower governor model limitations, necessitating separate consideration of inertia and PFR headroom. In contrast, modern systems with high renewable penetration and integrated battery energy storage system (BESS) present different dynamics, where BESS contributes to a rapid PFR. Thus, Eq. (4) in our study, which includes PFR headroom as a separate variable, captures the distinct influence of these factors on frequency nadir. In this way, we can obtain the frequency nadir constraint, which contains only a set of linear constraints to the MILP problem, resulting in a lower CoA than other methods, as shown in Section III-D. 2).

B. PROPOSED FNC-UC FRAMEWORK

Figure 1 shows the flow chart to obtain the LR-based frequency nadir constraint in the flow of the red arrows. First, a conventional one-year generation scheduling simulation is performed to obtain the generation dispatch of 365 days (8,760 hours). The network-constrained unit commitment is run sequentially for each day of this year. The Maui grid system and the time series of load and renewable power output are used for the one-year simulation. Then, after obtaining the generation dispatch of each hour, a dynamic simulation is performed to simulate the system frequency response following the trip of the generator with the most significant power output at that hour. The frequency nadir of each hour is obtained from this dynamic simulation. PSSE software is used for dynamic simulation in this study [41] because system operators and researchers for dynamic simulations of power systems use it extensively. Therefore, a linear regression model is proposed to obtain the relationship of the frequency nadir to the capacity of the most significant generation power output, the system inertia, and the PFR capacity/headroom of the system. Finally, a comprehensive techno-economic analysis is proposed to evaluate the proposed constraint by the 8760-hour simulation, assessing economic, reliability, and exceptional case factors. This analysis aims to analyze the performance and outcome of the proposed data-driven frequency nadir constraint. We conducted a comprehensive assessment of machine learning methods for estimating power system frequency nadir, taking into account loading levels, contingency types, and capacities. This work involved an extensive evaluation over a one-year duration, incorporating a wide range of load levels and capacity scenarios. Specifically, we focused on scenarios involving the contingency type of the largest generator tripping event, chosen strategically to represent a severe contingency in the power system. This deliberate emphasis on the largest generator tripping event allowed us to assess the effectiveness of the frequency nadir constraint in enhancing the system's resilience during critical incidents, establishing a robustness benchmark.

Our dataset, spanning one year and including diverse load and weather information, enabled us to explore a comprehensive array of capacity scenarios based on unit commitment. Figure 2 succinctly summarizes the performance results, demonstrating that linear regression consistently ranks third among various machine learning methods for estimating frequency nadir during the largest generator tripping event. Notably, the maximum absolute error of the linear regression model is a mere 0.0128 Hz, underscoring its remarkable accuracy and reliability in the estimation process.

III. UNIT COMMITMENT MODEL WITH FREQUENCY NADIR CONSTRAINT

This section introduces a unit commitment formulation with the proposed frequency nadir constraint and a minimum inertia constraint in addition to conventional unit commitment constraints.

A. OBJECTIVE FUNCTION

The objective of the FNC-UC problem includes the operating cost of traditional units—represented by their generation costs associated with their startup and shutdown costs—as well as the shortage penalties for the energy, regulation, and PFR services, as follows:

$$\min \sum_{t\in T}\sum_{i\in g}\left(SU_i u_{i,t} + SD_i w_{i,t} + cp_{i,t}\right) + LP * \Delta D_t + PFP * \Delta PFR_t + RP * (\Delta Reg_{u,t} + \Delta Reg_{d,t}) \quad (5)$$

$$cp_{i,t} = a_i v_{i,t} + b_i G_{i,t} + c_{i,t} G_{i,t}^2 \quad (6)$$

Note that the production cost, $cp_{i,t}$, of the traditional thermal unit shown in (5), can be approximated by a piecewise linear function from its quadratic production cost curve. In this model, we assume that the operational energy price of PV is 0. For ancillary services, the bidding prices are zero because the unit commitment model co-optimizes the energy and ancillary services, so the opportunity cost of providing ancillary services will be respected.

B. CONSTRAINTS FOR THE SINGLE UNIT

The constraints for traditional thermal units are similar to those in [42] and are presented as follows for completeness. We also consider the startup and shutdown trajectories of conventional generators in (9) and (10). In addition, (11)–(13) show the ramping rate constraint for units, and (14)–(18) impose limitations for ancillary services.

$$u_{i,t} + w_{i,t} \le 1 \quad (7)$$

$$v_{i,t} - v_{i,t-1} \le u_{i,t} - w_{i,t} \quad (8)$$

$$\sum_{\tau=t-T_{i,MinUp}+1}^{t} u_{i,t} \le v_{i,t} \quad (9)$$

$$\sum_{\tau=t-T_{i,MinDn}+1}^{t} w_{i,t} \le 1 - v_{i,t} \quad (10)$$

$$\overline{G_{i,t}} - G_{i,t-1} \leq R_i^U v_{i,t-1} + R_i^{SU} u_{i,t} \quad (11)$$

$$G_{i,t-1} - G_{i,t} \leq R_i^D v_{i,t} + R_i^{SD} w_{i,t} \quad (12)$$

$$\overline{G_{i,t}} \leq G_{i,t}^{max} v_{i,t} \quad (13)$$

$$G_{i,t} + Reg_{u,i,t} \leq \overline{G_{i,t+1}} \quad (14)$$

$$G_{i,t} + PFR_{i,t} \leq \overline{G_{i,t+1}} \quad (15)$$

$$G_{i,t} - Reg_{d,i,t} \geq G_{i,t+1}^{min} v_{i,t+1} \quad (16)$$

$$G_{i,t} + Reg_{u,i,t} - G_{i,t-1} \leq R_i^U \quad (17)$$

$$G_{i,t-1} - \left(G_{i,t} - Reg_{d,i,t}\right) \leq R_i^D \quad (18)$$

$$v_{i,t}, u_{i,t}, w_{i,t} \in \{0, 1\} \quad (19)$$

C. SYSTEM-WIDE CONSTRAINTS

The system constraints include the energy balance constraint for every time interval, the system regulation reserve, the PFR, and the transmission constraints, as follows:

$$\sum_{i \in g} \left(G_{i,t} + P_{p,t}\right) - \sum_{b \in B} D_{b,t} = 0 \quad (20)$$

$$D_{b,t} = \overline{D_{b,t}} - \Delta D_{b,t} \quad (21)$$

$$\Delta D_t = \sum_b \Delta D_{b,t} \quad (22)$$

$$\sum_{i \in g} PFR_{i,t} + \Delta PFR_t \geq PFR_t^r \quad (23)$$

$$\sum_{i \in g} Reg_{u,i,t} + \Delta Reg_{u,t} \geq Reg_{u,t}^r \quad (24)$$

$$\sum_{i \in g} Reg_{d,i,t} + \Delta Reg_{d,t} \geq Reg_{d,t}^r \quad (25)$$

$$-Limit_l \leq \sum_{i \in Lg} GSF_{l-i} \left(G_{i,t} + P_{p,t}\right) - \sum_{b \in Lb} GSF_{l-b} D_{b,t} \leq Limit_l \quad (26)$$

D. FREQUENCY NADIR CONSTRAINTS

1) MINIMAL INERTIA CONSTRAINT

Keeping inertia above a certain level is an intuitive method to maintain the frequency nadir for power systems with high penetration of renewable generation [43]; therefore, some power system operators in the United Kingdom deploy a straightforward approach to maintain the stable system frequency response by imposing a minimum inertia requirement constraint in system operation [7]. Because the inertia of conventional generation units is a static parameter, they can provide inertia response when they are online; therefore, the system minimum inertia requirement constraint can be directly formulated as follows:

$$\sum_{i=1}^{N} H_i \geq H_{min} \quad (27)$$

where H_i is the inertia of the *i-th* generation unit, and H_{min} is the predefined minimum inertia level that the system must maintain. Note that this study has no inertia response from PV and batteries.

2) FREQUENCY NADIR CONSTRAINT

From the linear regression model, (4), presented in the previous section, a linear constraint representing the frequency nadir requirement can be added to the unit commitment model. The linear constraint of the frequency nadir is shown in (28):

$$a * Inertia + b * PFR_{headroom} + c * P_{max} + d \geq f_{threshold} \quad (28)$$

TABLE 2. Parameter values of the linear regression frequency nadir constraint for the island system studied .

Coefficients	Value
Inertia (a)	0.000847
PFR headroom total (*b*)	0.006293
Largest Pgen (*c*)	-0.04737
Intercept (*d*)	59.86421

Table 2 presents the values of the parameters *a, b, c,* and *d* for the Maui Island system. Positive values for *a* and *b* indicate that inertia and PFR headroom positively impact the frequency nadir. Conversely, the largest generation output capacity negatively affects the frequency of nadir. The parameter *c* plays a significant role in the linear regression-based nadir constraint. The threshold for $f_{threshold}$ in the island system is set above the first level of the UFLS scheme (assumed to be 59 Hz). Figure 3 illustrates the flowchart of the FNC-UC framework, with the linear regression model establishing the relationship between the frequency nadir and the significant generation capacity, system inertia, and PFR headroom (as in Eq. (4)). While this study focuses on an island system, it's important to note that the proposed framework is adaptable to various power system cases, including both island and traditional systems. Island systems often exhibit weaker characteristics due to limited external power support compared to traditional transmission grids. Future research could explore and evaluate the framework's applicability to different power system types, considering their unique characteristics, impacts, and efficiency. This adaptability broadens the framework's utility and contributes to a more comprehensive understanding of its potential across diverse power system scenarios. Further analysis of these parameters is presented in Section IV-C.

IV. CASE STUDIES

To illustrate the effectiveness of the proposed FNC-UC model, the Maui Island system is used in this study. Maui grid operators are integrating several large hybrid PV and battery power plants into their systems. The stability of the system will be simulated at high penetration levels of renewable generation, especially PV.

The Maui Island grid case with two PV-BESS plant projects is selected as our study case. It includes 23 thermal units with capacities ranging from 2.75 MW to 21.45 MW. Four wind power plants are modeled. Two existing utility-scale PV plants, with 2.87 MW each, are considered. The Maui grid model includes 61 aggregated distributed

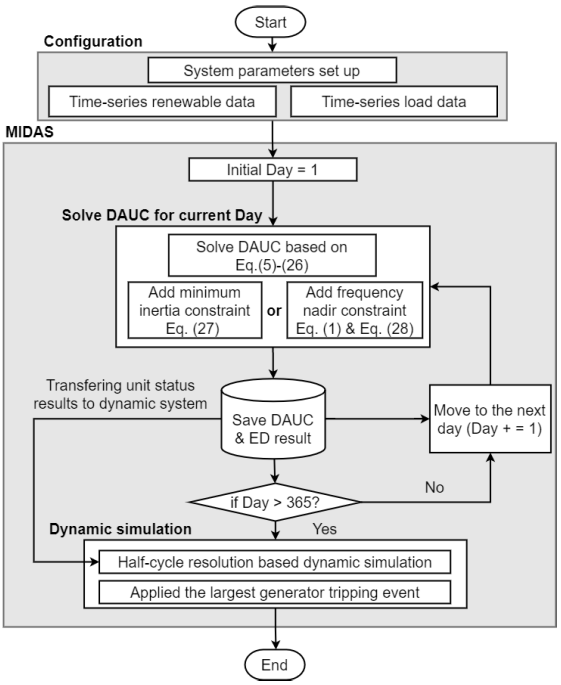

FIGURE 3. **Flowchart of the FNC-UC model.**

PV (DPV) units with a capacity of more than 140 MW. The DPV is not dispatchable, so the operator cannot curtail its power output. In contrast, the utility-scale PV is dispatchable, which means that its power output can be curtailed in real time; thus, the operator can curtail utility-scale PV but not DPV. The model has three large PV-BESS plants, representing the plant currently under development. The parameters of the three PV-BESS plants are summarized in Table 3. The PV-BESS plant model in our study represents a hybrid power plant where PV and BESS are integrated as a single unit within the power system. Specifically, we maintain the state of charge (SOC) at 50% by the end of each midnight, ensuring that it starts and ends each day at this level. This setup allows for flexibility in charging and discharging during the transition periods each day. Both the scheduling and dynamic simulations (in PSSE) incorporate the consistent PV-BESS model, reflecting realistic operational constraints and behaviors of the PV-BESS system. This approach ensures that SOC management is consistently represented throughout the study, providing insights into its impact on system dynamics and reliability. The generation mix is shown in Fig. 4. The 80-MW capacity of the utility PV includes the three PV-BESS plants. The yearly system load curve with hourly granularity is shown in Fig. 5. The system peak load is approximately 200 MW. The one-year simulation inherently encompasses various conditions, capturing a wide range of operational scenarios and their respective uncertainties.

The resolution of time in the FNC-UC is 1 hour, and the time span planned for the day in the FNC-UC is 24 hours. Regulation-down/-up requirements are assumed to be 3% of the system load. The PFR requirement is 4.75% of the system load. These numbers are chosen on the basis of the system's

TABLE 3. **Parameters of the PV-BESS plants.**

	Plant 1	Plant 2
Generator type	PV+BESS	PV+BESS
Rating	60 MW/240 MWh (split into two 30-MW/120-MWh units)	15 MW/60 MWh

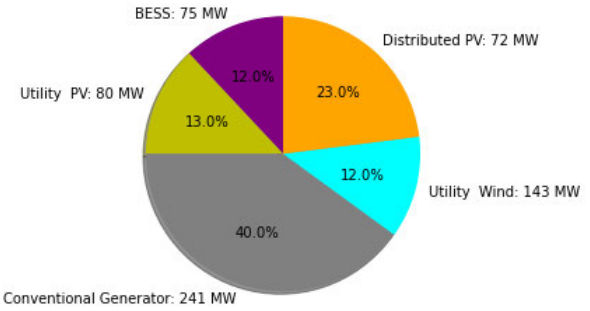

FIGURE 4. **Generation capacity mix in the island system.**

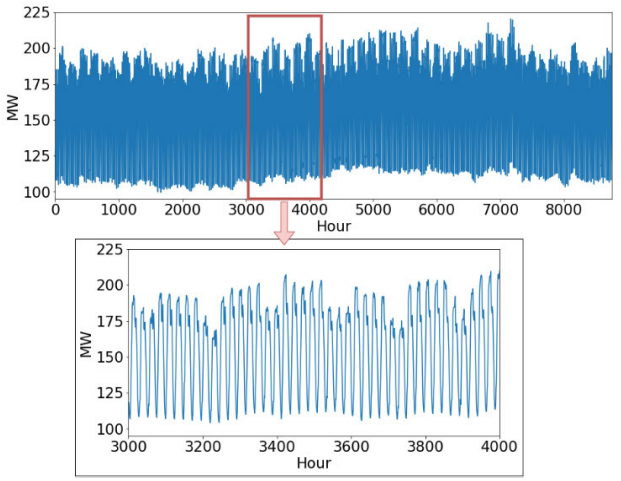

FIGURE 5. **Load curve in the simulated cases.**

dynamic simulation to maintain reliability. A detailed model of how to decide on the ancillary service requirements [42] is beyond the scope of this paper.

To evaluate the performance of the proposed FNC-UC model, three different cases are simulated to demonstrate the impacts of the frequency nadir constraints on the system generation scheduling and the system stability.

1) Case 1 (Baseline Case) is without a frequency nadir constraint.
2) Case 2 (Minimum Inertia Case) is with a minimum inertia requirement constraint (27). The operator historically used 350 MVA*s as the minimum inertia requirement in this island system. This inertia level was obtained from operational experience to limit the rate of change of frequency after the generation trip.
3) Case 3 (Nadir Constraint Case) is with a linear regression-based frequency nadir constraint (28)

but without the minimum inertia requirement constraint (27). The frequency nadir is chosen to be greater than 59 Hz, which is Maui grid's first UFLS frequency threshold.

In addition, the exceptional simulation results from those three cases are further analyzed in Subsection IV-C.

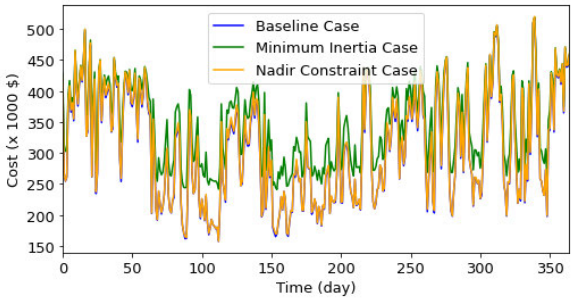

FIGURE 6. Annual generation cost of the three cases.

A. IMPACTS OF FREQUENCY NADIR CONSTRAINTS ON GENERATION SCHEDULING

The system daily generation costs versus the day of the year in the three cases are depicted in Fig. 6. The system generation cost with the minimum inertia constraint in Case 2 is higher than in the other two cases. Fig. 7 shows that the addition of the linear nadir constraint trivially increases the generation cost because the production cost curves of the Baseline Case and the linear regression-based Nadir Constraint Case are very close to each other; however, the constraint of the minimum inertia requirement significantly impacts the distribution of the daily generation costs. The minimum daily generation cost for the year with the minimum inertia requirement constraint (Case 2) is much higher than in the other two cases. Note that there is no comparably low cost (less than $250k) in the minimum inertia constraint because it has the restriction of maintaining enough inertia whether or not it is needed for that hour. Requiring a large amount of inertia leads to the introduction of more conventional generators online, resulting in a more expensive operating strategy. The higher system generation cost can be explained by investigating the detailed generation scheduling results in the three cases.

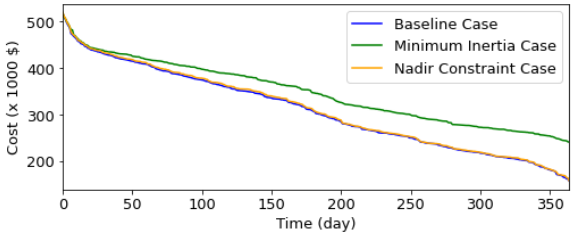

FIGURE 7. The generation cost duration of the three cases.

A five-day generation dispatch example for the three cases is shown in Fig. 8 to clarify the differences in generation

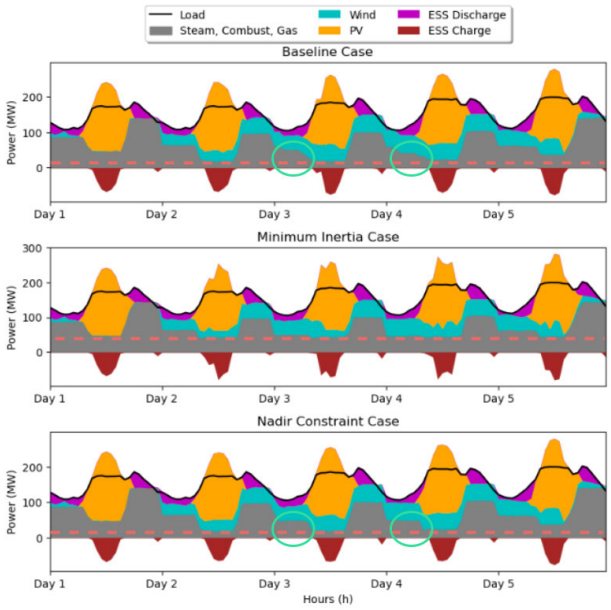

FIGURE 8. The five-day generation dispatch examples of the three cases.

scheduling. Purple and red represent the discharging and charging power of the BESS. Gray represents synchronous generation; orange and light blue represent PV and wind power, respectively. The red dashed line shows the lowest level of synchronous generation for each case. The minimum inertia requirement constraint maintains a higher inertia by bringing more synchronous generators online during the PV hours. Additionally, the green circles highlight the difference between the Baseline Case and the Nadir Constraint Case. The generation dispatches of most hours in these cases are similar, except when the BESS is discharging and PV is starting to ramp up. The BESS usually discharges during the time without PV generation while charging during the period with PV generation, as shown in Fig. 8. In addition, the BESS has a better capability of providing PFR, so allocating enough headroom for the BESS and committing more conventional generators helps maintain the frequency nadir of the power system. It can also be observed that this difference in the BESS scheduling leads to different wind and solar profiles because the charging of the BESS can impact the wind and solar curtailment in this island system with a high penetration level of hybrid power plants.

TABLE 4. One-year generation costs in the three cases.

	Baseline	Minimum Inertia	Nadir Constr.
Total cost	$112,997,029	$126,814,813	$113,864,047
% increase	–	12.23%	0.77%

The generation costs of the three cases are listed in Table 4. The cost of one-year generation in the baseline case is $112,997,029. Adding the frequency nadir constraint

costs 0.77% more than the baseline, while adding the minimum inertia requirement constraint costs 12.23% more than the baseline. The results in Figs. 6–8 and Table 4 demonstrate that the inclusion of the linear nadir constraint does not significantly increase the system generation cost. In contrast, the minimum-inertia requirement constraint significantly increases the generation operation cost. For the duration of this one-year simulation, a consistent fuel cost was maintained in the cost analysis. This methodological decision was crucial in ensuring the comparability of results. Moreover, the costs associated with the minimum inertia case were consistently higher than those in the other scenarios, a trend that held true regardless of supply curve variations while considering that fuel costs are the driver of generation costs. By maintaining constant fuel cost assumptions, our study provides a clear comparison of the economic impacts associated with those three cases.

B. IMPLICATION OF FREQUENCY NADIR CONSTRAINT ON STABILITY

This subsection demonstrates the efficacy of the proposed linear regression-based nadir constraint and the minimum-inertia requirement constraint in maintaining the frequency nadir. A PSSE validation and an analysis of the simulation results are shown in this subsection. Figure 9 shows the frequency nadir results of three cases over one year from the PSSE dynamic simulation. Note that the dynamic simulations in PSSE of the largest generator contingency (N-1) are built for each hour's generation schedule over one year (total of 8,760 snapshots). For each hour, the generator with the most significant power level is identified and tripped in the dynamic simulation. Figure 9 and Figure 10 demonstrate that adding a frequency nadir constraint, such as the linear regression-based nadir constraint or the minimum inertia constraint, can improve the system frequency nadir. Without these frequency nadir constraints, there is a risk that the frequency nadir is lower than the predefined 59-Hz UFLS threshold if the largest generator trips. Also, note that the minimum inertia constraint cannot guarantee that the frequency nadir of all hours is higher than 59 Hz. The system will still have a risk of a low-frequency nadir even with this minimum inertia requirement. On the contrary, with the proposed linear regression-based nadir constraint, the probability that the frequency nadir is lower than 59 Hz can be significantly reduced, as shown in Table 5. This demonstrates that the proposed nadir constraint performs better in this system than the minimum inertia requirement constraint previously considered by the operator.

The subplot of Fig. 9 shows the results for April. Both frequency constraints (Nadir Constraint Case and Minimum Inertia Case) help the system maintain a higher nadir than the Baseline Case; however, there are some green points (Minimum Inertia Case) approaching 60 Hz, and some orange points (Nadir Constraint Case) are below the corresponding blue points (Baseline Case). A detailed analysis of those situations appears in the following subsection.

A histogram of the simulation results reveals differences in distribution, as shown in Fig. 10. In the critical range of less

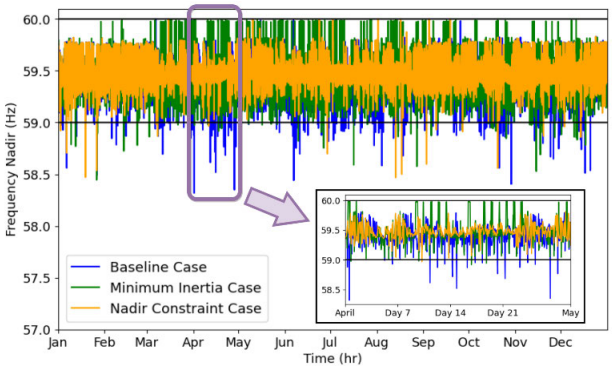

FIGURE 9. Frequency nadir for each hour of the year for the N-1 event.

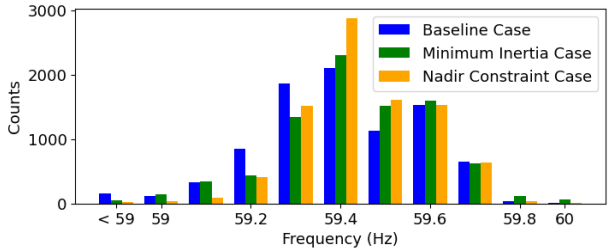

FIGURE 10. Frequency nadir distribution of the three cases.

than 59 Hz, the Baseline Case has 159 counts, the Minimum Inertia Case has 50 points, and the Nadir Constraint Case has 18 points, respectively. In other words, the Nadir Constraint Case performs best to improve the stability of the power system and reduce the risk of load shedding. The Minimum Inertia Case results in more nadirs in the range of [59.8, 60]; this will be discussed in the next section.

Table 5 shows the numbers of total hours and violation hours (in which the frequency < 59 Hz) as well as the percentage of hours that result in violations in the three cases. The Baseline Case has the highest probability of a frequency nadir lower than 59 Hz among the three cases, at 1.8%. The minimum inertia case has a probability of 0. 57%, and the linear regression-based Nadir constraint case has a probability of 0. 2% of frequency violation of the nadir in the most severe dynamic simulation of N-1 contingency.

TABLE 5. Probabilities of frequency nadir lower than 59 Hz in the three cases.

	Baseline	Min. Inertia	Nadir Const.
Total hours	8760	8760	8760
Violation hrs	159	50	18
Probability	1.8%	0.57%	0.20%

Figure 11 shows the number of times when the nadir is less than 59 Hz for each hour of the day. Without a frequency nadir constraint, most hours of the day have a risk of a frequency nadir lower than 59 Hz, as shown in the

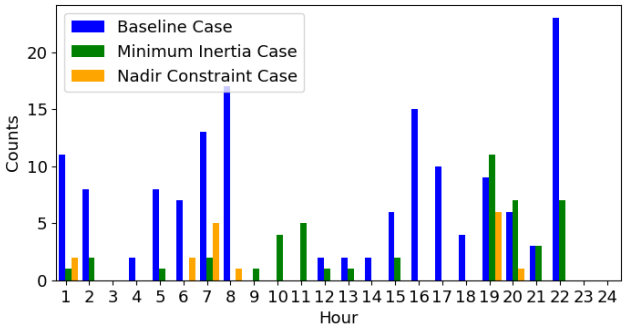

FIGURE 11. **Hourly counts of the frequency nadir lower than 59 Hz in the three cases.**

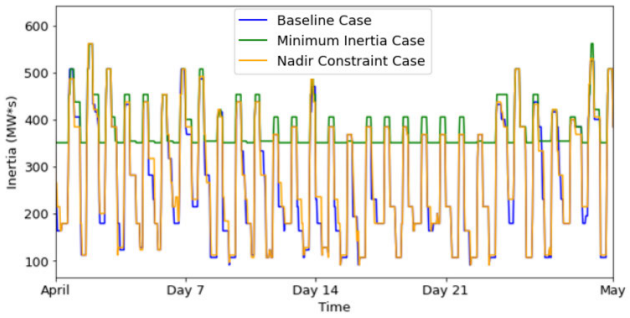

FIGURE 12. **The system scheduled one-month total inertia in the three cases.**

Baseline Case. After adding the linear regression-based nadir constraint, there are only a few hours when the frequency has a risk of falling lower than 59 Hz. The minimum inertia constraint is also helpful in reducing this risk, but is not as beneficial as the linear regression-based nadir constraint. This figure also shows that in the Maui Island system with a high penetration level of hybrid power plants (PV plus battery energy storage), the risk of a low nadir occurs mostly during non-PV hours. The main reason is that during these non-PV hours, the BESS discharges to satisfy the load in the system; thus, the headroom of the batteries reduces during these hours. Consequently, the system has a smaller PFR headroom from the batteries; therefore, these hours have a relatively high risk of a lower nadir. In contrast, during the day (PV hours), the BESS is charging, which leads to ample PFR headroom from the batteries because a BESS can change from charging to discharging to provide a large capacity of PFR if needed. This is an exciting phenomenon in the island system with a high penetration of hybrid power plants. In large interconnected systems with high PV penetration levels, the risk of a low nadir usually occurs around noon, when the PV penetration level is high, and the system has a low inertia level. This demonstrates that the proposed nadir constraint will not significantly increase the system generation cost but can dramatically improve the system frequency nadir; therefore, the proposed nadir constraint is promising in the actual operation of this island system.

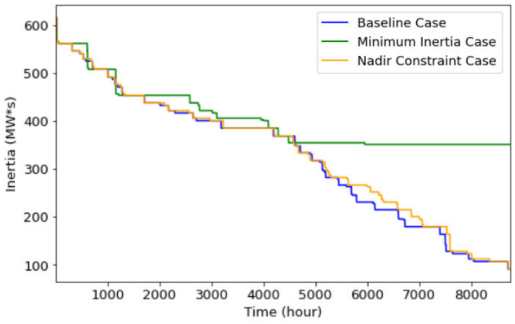

FIGURE 13. **The inertia duration curves in the three cases.**

TABLE 6. **System inertia metrics for the three cases (MW*s).**

	Baseline	Minimum Inertia	Nadir Constr.
Avg. inertia	326.4	**404.6**	332.3
Max. inertia	615.8	615.8	615.8
Min. inertia	91.35	**351.1**	91.35

The one-month system scheduled inertia and the one-year inertia duration curve are shown in Fig. 12 and Fig. 13, respectively. The minimum inertia requirement frequently results in system inertia that is always higher than in the Baseline Case. In contrast, the nadir constraint does not significantly increase the system inertia. This is also shown in Table 6. The maximum inertia levels of the three cases are the same. The minimum inertia levels of the Baseline Case and the Nadir Constraint Case are the same. In contrast, the Minimum Inertia Case has a higher minimum inertia level, as the constraint requires. The average inertia levels of the Baseline Case and the Nadir Constraint Case are very close. This is because the nadir constraint can schedule more PFR headroom instead of requiring more thermal units online for most hours, leading to a generation cost similar to the Baseline Case.

C. EXCEPTIONAL CASE ANALYSIS

This subsection analyzes two exceptional situations mentioned in the simulation results of the previous subsections, i.e., 1) the Minimum Inertia Case's frequency nadir close to 60 Hz and 2) a lower frequency nadir that occurred after adding the nadir constraint compared to the Baseline Case. The main reasons for two counterintuitive situations are discussed here:

1) FREQUENCY NADIR of MINIMUM INERTIA CASE IS NEAR 60 Hz

Three examples are selected in Table 7 where the frequency nadir is near 60 Hz after the largest N-1 generation contingency in the Minimum Inertia Case. In all these cases, the BESS is charging, which means they consume power; therefore, once the most significant generation (much smaller than the total charging power) is tripped, the BESS can immediately stop charging (consuming power) to compensate

TABLE 7. Nadir near 60 Hz in the minimum inertia constraint case.

ID	Max Pgen (MW)	PFR (MW)	Inertia (MW*s)	BESS HR (MW)	Est. Nadir (Hz)	Act. Nadir (Hz)
1	19.04	1.81	351.1	128.3	59.31	59.82
2	16.87	1.80	354.5	119.2	59.42	59.73
3	18.53	1.81	354.5	140.3	59.33	59.90

for the tripped generation. Note that the BESS headroom (HR) is the difference between its present power level and its maximum power output, which is greater than its rating if it is charging because the current power level is negative when charging. Observe that the highest BESS headroom results in the highest actual frequency nadir among those examples. In addition, the inertia in the system in these hours (because of the minimum inertia constraint) helps prevent a sudden drop in frequency. The BESS's high inertia and great charging power result in high-frequency nadirs in the Minimum Inertia Case.

TABLE 8. Nadir constraint case has a lower nadir than the baseline case.

ID	Case	Max Pgen (MW)	PFR (MW)	Inertia (MW*s)	BESS HR (MW)	Est. Nadir (Hz)	Act. Nadir (Hz)
1	**Baseline**	31.1	1.54	384.8	35.5	58.72	59.01
	Nadir Constr.	20	1.54	384.8	11.2	59.25	58.47
2	**Baseline**	31.1	1.81	453.6	25.7	58.80	59.02
	Nadir Constr.	26.2	1.96	453.6	20.2	59.01	58.92

2) LINEAR REGRESSION-BASED NADIR CONSTRAINT CASE HAS LOWER FREQUENCY NADIR THAN BASELINE

Table 8 shows the cases where the baseline has a higher frequency nadir than those with a frequency nadir constraint. The examples occurred on day 2, hour 19, and day 6, hour 19, respectively. These are both non-PV periods when a BESS is tripped as the largest generator. As shown in the first example, the predicted frequency nadirs from the linear regression method are 58.92 Hz and 59.25 Hz for the Baseline Case and the Nadir Constraint Case, respectively; thus, the estimated system frequency nadir is higher than the predetermined level of 59 Hz in the frequency-constrained case. However, the actual frequency nadirs simulated via PSSE are 59.01 (Baseline) and 58.47 Hz (Nadir-Constrained). In the Baseline Case, a BESS with a generation of 31.1 MW is tripped, and there is 35.5 MW of headroom in the remaining BESS; in contrast, 20 MW of generation is tripped in the frequency Nadir Constraint Case, but there is only 11.2 MW of headroom in the remaining BESS. In these cases, the BESS is a primary provider of PFR. If the remaining BESS has smaller PFR headroom, it leads to a lower frequency nadir. In other words, a considerable value of BESS headroom represents a better ability of the BESS to respond to the frequency drop; therefore, when the BESS is enabled to provide a fast frequency response, the risk that a BESS trip should be considered in the system operation.

Additionally, in Fig. 9, an interesting observation emerges where the minimum inertia case exhibits a lower frequency nadir than the frequency nadir constraint case. This finding suggests that while inertia is indeed a significant factor in determining power system frequency nadir, it is not the sole determinant. Our analysis reveals that increasing inertia alone is not the exclusive solution. Several factors, including reserve capacity and the influence of the largest generator, play crucial roles in shaping the frequency nadir. A direct comparison between the minimum inertia case and the frequency nadir constraint case highlights noteworthy patterns. Firstly, the minimum inertia case generally exhibits higher inertia levels compared to other scenarios. This consistent trend suggests that while inertia contributes significantly to system stability, its impact is nuanced and influenced by other system parameters. Secondly, there are instances where, despite a system with large inertia, the BESS headroom is relatively small, leading to a weaker frequency response. Additionally, limitations imposed by the frequency nadir constraint on the largest generator significantly contribute to achieving a higher frequency nadir in comparison to the minimum inertia case. Figure 12 illustrates these instances, underscoring the complexity of power system dynamics, where multiple factors, including reserve capacity, BESS headroom, and generator constraints, collectively shape the system's frequency response rather than inertia alone.

V. CONCLUSION

To maintain the frequency nadir of a future grid, especially an island grid with high penetration levels of renewable generation, this paper proposes a linear regression-based frequency nadir constraint in the unit commitment problem. The frequency nadir of the largest generation trip event is considered endogenously in the generation scheduling stage. Simulation results demonstrate that the frequency nadir of the system can improve significantly with this nadir constraint in a realistic island system. Therefore, the risk of a frequency nadir lower than the predetermined threshold is reduced. Furthermore, compared to the direct minimum inertia requirement constraint, the proposed linear regression-based nadir constraint trivially increases the system generation cost while achieving a better nadir response; therefore, the proposed nadir constraint can serve as a good reference for future system operation with high penetration levels of hybrid PV and battery resources.

Future work will include testing other data-driven models to improve the forecast accuracy of the proposed nadir constraint. More hybrid plant operational strategies will be investigated considering the frequency nadir risk. Another future research direction can address the complexities introduced by the virtual inertia of IBRs, specifically those with Grid-Forming Inverters in the frequency nadir constraint.

ACKNOWLEDGMENT

The views expressed in the article do not necessarily represent the views of the DOE or the U.S. Government. The U.S.

REFERENCES

[1] Z. Zhang, E. Du, F. Teng, N. Zhang, and C. Kang, "Modeling frequency dynamics in unit commitment with a high share of renewable energy," *IEEE Trans. Power Syst.*, vol. 35, no. 6, pp. 4383–4395, Nov. 2020.

[2] S. Dong, X. Fang, J. Tan, N. Gao, X. Cui, and A. Hoke, "A unified analytical method to quantify three types of fast frequency response from inverter-based resources," in *Proc. 22nd Wind Solar Integr. Workshop*, 2023, pp. 669–674.

[3] X. Fang, H. Yuan, and J. Tan, "Secondary frequency regulation from variable generation through uncertainty decomposition: An economic and reliability perspective," *IEEE Trans. Sustain. Energy*, vol. 12, no. 4, pp. 2019–2030, Oct. 2021.

[4] N. Gao, S. Dong, X. Fang, A. Hoke, D. W. Gao, and J. Tan, "Developing frequency stability constraint for unit commitment problem considering high penetration of renewables," in *Proc. IEEE 50th Photovolt. Spec. Conf. (PVSC)*, Sep. 2023, pp. 1–4.

[5] V. V. Terzija, "Adaptive underfrequency load shedding based on the magnitude of the disturbance estimation," *IEEE Trans. Power Syst.*, vol. 21, no. 3, pp. 1260–1266, Aug. 2006.

[6] N. Gao, D. W. Gao, and X. Fang, "Manage real-time power imbalance with renewable energy: Fast generation dispatch or adaptive frequency regulation?" *IEEE Trans. Power Syst.*, vol. 38, no. 6, pp. 5278–5289, Jun. 2023.

[7] A. Grundy. *National Grid Eso Claims World First Approach To Inertia, Awarding $328 m in Contracts*. Accessed: Nov. 22, 2022. [Online]. Available: https://www.current-news.co.uk/news/national-grid-eso-claims-world-first-approach-to-inertia-awarding-328m-in-contracts

[8] G. W. Chang, C.-S. Chuang, T.-K. Lu, and C.-C. Wu, "Frequency-regulating reserve constrained unit commitment for an isolated power system," *IEEE Trans. Power Syst.*, vol. 28, no. 2, pp. 578–586, May 2013.

[9] H. Ahmadi and H. Ghasemi, "Security-constrained unit commitment with linearized system frequency limit constraints," *IEEE Trans. Power Syst.*, vol. 29, no. 4, pp. 1536–1545, Jul. 2014.

[10] L. E. Sokoler, P. Vinter, R. Bærentsen, K. Edlund, and J. B. Jørgensen, "Contingency-constrained unit commitment in meshed isolated power systems," *IEEE Trans. Power Syst.*, vol. 31, no. 5, pp. 3516–3526, Sep. 2016.

[11] Y. Wen, W. Li, G. Huang, and X. Liu, "Frequency dynamics constrained unit commitment with battery energy storage," *IEEE Trans. Power Syst.*, vol. 31, no. 6, pp. 5115–5125, Nov. 2016.

[12] F. Teng, V. Trovato, and G. Strbac, "Stochastic scheduling with inertia-dependent fast frequency response requirements," *IEEE Trans. Power Syst.*, vol. 31, no. 2, pp. 1557–1566, Mar. 2016.

[13] V. Trovato, A. Bialecki, and A. Dallagi, "Unit commitment with inertia-dependent and multispeed allocation of frequency response services," *IEEE Trans. Power Syst.*, vol. 34, no. 2, pp. 1537–1548, Mar. 2019.

[14] L. Badesa, F. Teng, and G. Strbac, "Simultaneous scheduling of multiple frequency services in stochastic unit commitment," *IEEE Trans. Power Syst.*, vol. 34, no. 5, pp. 3858–3868, Sep. 2019.

[15] P. Rabbanifar and N. Amjady, "Frequency-constrained unit-commitment using analytical solutions for system frequency responses considering generator contingencies," *IET Gener., Transmiss. Distrib.*, vol. 14, no. 17, pp. 3548–3560, Sep. 2020, doi: 10.1049/iet-gtd.2020.0097.

[16] L. Liu, Z. Hu, X. Duan, and N. Pathak, "Data-driven distributionally robust optimization for real-time economic dispatch considering secondary frequency regulation cost," *IEEE Trans. Power Syst.*, vol. 36, no. 5, pp. 4172–4184, Sep. 2021.

[17] S. S. Oskouee, S. Kamali, and T. Amraee, "Primary frequency support in unit commitment using a multi-area frequency model with flywheel energy storage," *IEEE Trans. Power Syst.*, vol. 36, no. 6, pp. 5105–5119, Nov. 2021.

[18] T. Ding, Z. Zeng, M. Qu, J. P. S. Catalao, and M. Shahidehpour, "Two-stage chance-constrained stochastic thermal unit commitment for optimal provision of virtual inertia in wind-storage systems," *IEEE Trans. Power Syst.*, vol. 36, no. 4, pp. 3520–3530, Jul. 2021.

[19] K. Li, H. Guo, X. Fang, S. Liu, F. Teng, and Q. Chen, "Market mechanism design of inertia and primary frequency response with consideration of energy market," *IEEE Trans. Power Syst.*, early access, Nov. 21, 2022, doi: 10.1109/TPWRS.2022.3223497.

[20] S. Jiang et al., "A novel robust frequency-constrained unit commitment model with emergency control of HVDC," *Energy Rep.*, vol. 8, pp. 15729–15739, Nov. 2022. [Online]. Available: https://www.sciencedirect.com/science/article/pii/S2352484722026695

[21] D. Ortiz-Villalba, J. Llanos, Y. Muñoz-Jadan, R. Moreno, C. Rahmann, and B. C. Pal, "Optimizing system operation with nadir considerations via simulations of detailed system dynamic responses," *Electr. Power Syst. Res.*, vol. 212, Nov. 2022, Art. no. 108533. [Online]. Available: https://www.sciencedirect.com/science/article/pii/S0378779622006393

[22] C. Zhao and Y. Guan, "Data-driven stochastic unit commitment for integrating wind generation," *IEEE Trans. Power Syst.*, vol. 31, no. 4, pp. 2587–2596, Jul. 2016.

[23] Z. Jin, K. Pan, L. Fan, and T. Ding, "Data-driven look-ahead unit commitment considering forbidden zones and dynamic ramping rates," *IEEE Trans. Ind. Informat.*, vol. 15, no. 6, pp. 3267–3276, Jun. 2019.

[24] T. Ding et al., "Duality-free decomposition based data-driven stochastic security-constrained unit commitment," *IEEE Trans. Sustain. Energy*, vol. 10, no. 1, pp. 82–93, Jan. 2019.

[25] D. T. Lagos and N. D. Hatziargyriou, "Data-driven frequency dynamic unit commitment for island systems with high RES penetration," *IEEE Trans. Power Syst.*, vol. 36, no. 5, pp. 4699–4711, Sep. 2021.

[26] Y. Zhang et al., "Encoding frequency constraints in preventive unit commitment using deep learning with region-of-interest active sampling," *IEEE Trans. Power Syst.*, vol. 37, no. 3, pp. 1942–1955, May 2022.

[27] L. Yang, Z. Li, Y. Xu, J. Zhou, and H. Sun, "Frequency constrained scheduling under multiple uncertainties via data-driven distributionally robust chance-constrained approach," *IEEE Trans. Sustain. Energy*, vol. 14, no. 2, pp. 763–776, Apr. 2023.

[28] Y. Shen, W. Wu, B. Wang, Y. Yang, and Y. Lin, "Data-driven convexification for frequency nadir constraint of unit commitment," *J. Mod. Power Syst. Clean Energy*, vol. 11, pp. 1–7, Jan. 2022.

[29] M. Rajabdorri, E. Lobato, and L. Sigrist, "Robust frequency constrained uc using data driven logistic regression for island power systems," *IET Gener., Transmiss. Distrib.*, vol. 16, no. 24, pp. 5069–5083, Dec. 2022, doi: 10.1049/gtd2.12658.

[30] Y. Su et al., "An adaptive PV frequency control strategy based on real-time inertia estimation," *IEEE Trans. Smart Grid*, vol. 12, no. 3, pp. 2355–2364, May 2021.

[31] H. Li, Y. Qiao, Z. Lu, B. Zhang, and F. Teng, "Frequency-constrained stochastic planning towards a high renewable target considering frequency response support from wind power," *IEEE Trans. Power Syst.*, vol. 36, no. 5, pp. 4632–4644, Sep. 2021.

[32] X. Liu et al., "A comparison of machine learning methods for frequency nadir estimation in power systems," in *Proc. IEEE Kansas Power Energy Conf. (KPEC)*, Manhattan, KS, USA, Apr. 2022, pp. 1–5.

[33] J. Tan. (2023). *Final Technical Report: Multi-Timescale Integrated Dynamics and Scheduling for Solar (MIDAS-Solar)*. [Online]. Available: https://www.osti.gov/biblio/1972321

[34] *NREL: Multi-timescale Integrated Dynamic and Scheduling*. Accessed: Sep. 16, 2022. [Online]. Available: https://www.nrel.gov/grid/midas.html

[35] P. Kundur, *Power System Stability and Control*, M. Lauby, Ed. New York, NY, USA: McGraw-Hill, 1994.

[36] H. Chávez, R. Baldick, and S. Sharma, "Governor rate-constrained OPF for primary frequency control adequacy," *IEEE Trans. Power Syst.*, vol. 29, no. 3, pp. 1473–1480, May 2014.

[37] Y.-Y. Lee and R. Baldick, "A frequency-constrained stochastic economic dispatch model," *IEEE Trans. Power Syst.*, vol. 28, no. 3, pp. 2301–2312, Aug. 2013.

[38] I. Goodfellow, Y. Bengio, and A. Courville, *Deep Learning*. Cambridge, MA, USA: MIT Press, 2016. [Online]. Available: http://www.deeplearningbook.org

[39] S. Rath, A. Tripathy, and A. R. Tripathy, "Prediction of new active cases of coronavirus disease (COVID-19) pandemic using multiple linear regression model," *Diabetes Metabolic Syndrome, Clin. Res. Rev.*, vol. 14, no. 5, pp. 1467–1474, Sep. 2020.

[40] C. B. Santiago, J.-Y. Guo, and M. S. Sigman, "Predictive and mechanistic multivariate linear regression models for reaction development," *Chem. Sci.*, vol. 9, no. 9, pp. 2398–2412, 2018.

[41] *PSS®E—Transmission Planning and Analysis—PSS®Power System Simulation and Modeling Software—Siemens Global*. Accessed: Sep. 18, 2022. [Online]. Available: https://new.siemens.com/global/en/products/energy/energy-automation-and-smart-grid/pss-software/pss-e.html
[42] E. Ela, M. Milligan, and B. Kirby, "Operating reserves and variable generation," Dept. Nat. Renew. Energy Lab., Golden, CO, USA, Tech. Rep. NREL/TP-5500-51978, 2011.
[43] P. Denholm, T. Mai, R. Kenyon, B. Kroposki, and M. O'Malley, "Inertia and the power grid: A guide without the spin," Dept. Nat. Renewable Energy Lab., Golden, CO, USA, Tech. Rep. NREL/TP-6120-73856, 2020.

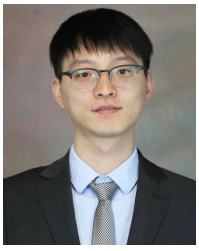

XUEBO LIU (Graduate Student Member, IEEE) received the B.S. degree in electrical and computer engineering from Kansas State University, Manhattan, KS, USA, in 2020, where he is currently pursuing the Ph.D. degree in electrical and computer engineering. His current research interests include building energy management systems, machine learning, optimizing, and modeling in renewable energy.

XIN FANG (Senior Member, IEEE) received the B.S. degree from Huazhong University of Science and Technology, Wuhan, China, in 2009, the M.S. degree from China Electric Power Research Institute, Beijing, China, in 2012, and the Ph.D. degree from The University of Tennessee (UTK), Knoxville, TN, USA, in 2016. He is currently an Assistant Professor with the Department of Electrical and Computer Engineering, Mississippi State University (MSU). Before joining MSU, he was a Senior Researcher with the National Renewable Energy Laboratory (NREL) from 2017 to 2022. His research interests include power system planning and operation, electricity market operation considering renewable energy integration, and cyber-physical transmission and distribution modeling and simulation. He is an Associate Editor of IEEE TRANSACTIONS ON POWER SYSTEMS and IEEE TRANSACTIONS ON SUSTAINABLE ENERGY.

NINGCHAO GAO (Graduate Student Member, IEEE) received the M.S. degree from North China Electric Power University, Beijing, China, in 2012, and the Ph.D. degree from the University of Denver, Denver, CO, USA, in 2023. Before joining the University of Denver, she was a Power System Engineer with Shanghai Electric Power Company of State Grid Corporation of China. She is currently a Post-Doctoral Researcher with the National Renewable Energy Laboratory (NREL). Her research interests include power system frequency stability analysis with large-scale renewable energy integration, load prediction based on machine learning methods, and power system economic analysis.

HAOYU "HARRY" YUAN (Member, IEEE) received the Ph.D. degree from The University of Tennessee, Knoxville, TN, USA, in 2016. Since 2021, he has been trading in U.S. Electric Market. He is currently a power trader at a private hedge fund. Prior to his career in power trading, he was a Research Engineer with the National Renewable Energy Laboratory with a research focus on integrating large-scale renewable energy into bulk electric systems. He was also employed at Peak Reliability where he was the key technical person involved in developing and maintaining control room applications and operation planning tools in U.S. Western Interconnection.

ANDY HOKE (Senior Member, IEEE) received the M.S. and Ph.D. degrees in electrical, computer, and energy engineering from the University of Colorado at Boulder, Boulder, CO, USA, in 2013 and 2016, respectively. He is currently a Principal Engineer with the Power Systems Engineering Center, National Renewable Energy Laboratory (NREL), where he has worked for the past 14 years. His expertise is in grid integration of power electronics and inverter-based renewable and distributed energy. His research interests include advanced inverter control design, hardware-in-the-loop testing and model development, power systems modeling and simulation, and standards development. He is a Registered Professional Engineer in the State of Colorado. He has served as the Chair of IEEE 1547.1 and P2800.2, which contain the test and verification procedures to ensure DERs and inverter-based resources conform to the grid interconnection requirements of IEEE Standards 1547 and 2800, respectively.

HONGYU WU (Senior Member, IEEE) received the B.S. degree in energy and power engineering and the Ph.D. degree in control science and engineering from Xi'an Jiaotong University, China. He is currently a Lucas-Rathbone Professor and a Steve Hsu Keystone Research Scholar with the Mike Wiegers Department of Electrical and Computer Engineering, Kansas State University. Before joining Kansas State University, he was a Research Engineer with the Power Systems Engineering Center, National Renewable Energy Laboratory. His research interests include grid integration of renewable energy, cyber-physical security of smart grids, power system planning and operation, and building energy management. He was a recipient of the National Science Foundation (NSF) Career Award. He is an Associate Editor of IEEE TRANSACTIONS ON SMART GRID and IEEE TRANSACTIONS ON INDUSTRIAL INFORMATICS.

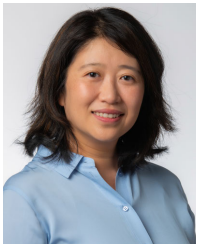

JIN TAN (Senior Member, IEEE) received the B.E. and Ph.D. degrees in electrical engineering from Southwest Jiaotong University, Chengdu, China, in 2007 and 2014, respectively. From 2009 to 2011, she was a Visiting Ph.D. Student with the Department of Energy Technology, Aalborg University, Denmark. In 2014, she was a Post-Doctoral Researcher with the Department of Electrical Engineering and Computer Science, The University of Tennessee, Knoxville, TN, USA. She is currently a Principal Engineer and a Distinguished Member of the Research Staff with the Power Systems Engineering Center, National Renewable Energy Laboratory, Golden, CO, USA. She has more than ten years of experience in large-scale renewable integration studies. Her research interests include power system stability and control with large-scale renewable integration, multi-timescale modeling and simulation of inverter-based resources in grids, and energy storage for grid applications.